Superalloys 2008
Roger C. Reed, Kenneth A. Green, Pierre Caron, Timothy P. Gabb, Michael G. Fahrmann, Eric S. Huron and Shiela A. Woodard
TMS (The Minerals, Metals & Materials Society), 2008

A STUDY OF HAZ MICROFISSURING IN A NEWLY DEVELOPED ALLVAC® 718 PLUS ™ SUPERALLOY

Krutika Vishwakarma, Mahesh Chaturvedi
Department of Mechanical and Manufacturing Engineering,
University of Manitoba, Winnipeg, Canada. R3T5V6

Keywords: HAZ micro-fissuring, Allvac® 718 PLUS™ (718 Plus), Gleeble hot ductility measurements, SIMS analysis, Inconel 718

Abstract

Allvac® 718 PLUS™ (718 Plus) is a newly developed γ′ strengthened Ni-base superalloy with superior high temperature properties compared to its baseline superalloy, Inconel 718, but only limited information about its weldability is available. Electron beam welding response of this new superalloy was studied in two different pre-weld heat treated conditions. Microstructural characterization, prior to and after bead-on-plate electron beam welding, was done by optical microscopy, scanning electron microscopy and transmission electron microscopy. Two versions of 718 Plus with different concentrations of boron and phosphorus were investigated to study the effect of minor alloying elements on weldability. Grain boundary segregation of these minor alloying elements was studied using Secondary Ion Mass Spectrometer (SIMS). HAZ cracking due to liquation at the grain boundaries was observed in the alloys. The welding response of 718 Plus alloys was compared with that of Inconel 718 using two weldability evaluation techniques viz. – weld crack measurements in actual welds and hot-ductility measurements using Gleeble thermo-mechanical simulator. The results obtained by both the techniques were in agreement with each other and indicated that weldability of Inconel 718 was slightly better than that of 718 Plus alloy with normal boron and phosphorus concentration, although weldability of the higher boron and phosphorus version of 718 Plus alloy deteriorated significantly. The causes of cracking in 718 Plus alloys and the parameters affecting it are discussed and the welding response of the newly developed superalloy is assessed.

Introduction

Superalloys are used in high temperature components of land and aero based gas turbines. The ever increasing demand for more power efficient gas turbines is encouraging the development of superalloys with higher working temperature and better stability in harsh operating environments. In spite of superior properties of today's superalloys, gas turbine components do suffer wear and tear, and it is economically more viable to repair them than to replace them. Fusion welding is one of the most commonly used techniques to repair the worn out parts. Unfortunately these high temperature components are generally difficult to weld and suffer from weld cracking in the fusion and heat affected zone which could render them unsuitable for further use. Weld cracking is also encountered during manufacturing of these components. This problem is commonly associated with Ni-base superalloys strengthened by ordered FCC intermetallic strengthening precipitate, γ′ [1]. On the other hand, Ni-Fe base superalloys, like Inconel 718, which are strengthened by BCT γ″ precipitate, show better resistance to repair welding but cannot be used beyond 650°C due to the metastable nature of γ″ [2]. Considerable research was done to stabilize γ″ precipitate to temperature higher than 650°C, beyond which it transforms to orthorhombic needle like δ phase [3-5]. Nevertheless, the operating temperatures could not be raised to match those of other γ′ strengthened alloys. Recently, a new superalloy was developed by ATI ALLVAC Inc., Allvac®718 PLUS™ (718 Plus) based on Inconel 718, but primarily strengthened by γ′ precipitate [6]. 718 Plus alloy has superior high temperature properties than those of other γ′ strengthened alloys like Waspaloy and has a working temperature advantage of 55°C over Inconel 718. As limited information about physical metallurgy and weldability of this new superalloy exists in open literature; a project was initiated to understand its electron beam welding response and compare it with its baseline superalloy.

Weld cracking in a material depends on the combination of mechanical (restraint, sample geometry, etc.) and metallurgical factors (composition, heat treatment, microstructure, etc.). Generally the mechanical factors are difficult to control and hence metallurgical factors are altered to enhance resistance towards cracking. Microstructure of the alloy is one of the most important metallurgical factors that affect weldability and it is imperative to characterize it. Hence, characterization of microstructure prior to and after welding forms the basis of this weldability study.

The effect of minor alloying elements on the weldability of superalloys is well reported in literature [7-10] and it is established that grain boundary segregation of certain melting point depressing elements can significantly impact the resistance to cracking. Elements likes sulphur [8, 10], boron [11, 12], phosphorus [10] and carbon [9] are known to adversely affect weldability of Inconel 718. To study the effect of boron and phosphorus on the weldability of 718 Plus alloys, two versions of 718 Plus with varying amounts of boron and phosphorus were used in this study. Grain boundary segregation in 718 Plus alloys was studied by Secondary Ion Mass Spectrometer (SIMS).

In addition, weldability of 718 Plus alloy was also compared to that of the well established baseline superalloy Inconel 718. The evaluation of weldability was done by two techniques – crack length measurements in the actual welds and hot ductility measurements by Gleeble thermo-mechanical simulator.

Materials and Experimental

Hot rolled wrought plates, and 10mm diameter by 150 mm long threaded rods, the latter for hot ductility testing by Gleeble machine, of the three alloys viz., Inconel 718, 718 Plus HC-20 with normal B and P concentrations and 718 Plus HC-49 with higher B and P were supplied by ATI ALLVAC Inc. The chemical composition of these alloys is given in Table 1. 12.7 mm × 12.7 mm × 101.6 mm sections were cut from the wrought plates and, along with the Gleeble specimens, were given the standard

commercial solution heat treatment of 950°C for 1 hr followed by water quenching. This treatment dissolved all the main precipitates, except the grain boundary δ phase, in the three alloys. To obtain an essentially single phase material, which is often desirable for welding, the alloys were solution heat treated at 1050°C for 1hr followed by water quenching. Autogenous bead-on-plate electron beam welds were made on the solution heat treated plates using 44KV voltage, 79mA current and 152 cm/min speed. Metallographic specimens were etched either by modified Kalling's reagent or electrolytically in 10% oxalic acid. The fusion zone and HAZ microstructures were examined and analyzed by optical microscope, JEOL 5900 Scanning electron microscope (SEM) equipped with an ultra thin window Oxford energy dispersive spectrometer (EDS) and JEOL 2000 FX TEM equipped with EDAX ultra thin window detector. X-ray microanalysis in TEM, using theoretical Cliff-Lorimer k factors, and selected area diffraction analysis were performed on interdendritic constituents extracted on carbon extraction replicas and on those present in thin foils prepared from weld fusion zone. Extraction replicas were prepared through standard technique with a solution of 10 ml HCl and 1 g tartaric acid in 90 ml methanol at 4 V. Thin foils were produced by twin-jet polishing with 10% perchloric acid in 90% methyl alcohol at -20 to -30°C temperature, 1.5 A current and 2 V voltage. Grain boundary segregation was examined by Cameca IMS-7f magnetic sector Secondary Ion Mass Spectrometer. Positive secondary ion images of $11B^+$ and negative secondary ion images of $31P^-$ were acquired in microscopy mode by means of 1nA or 300 pA O_2^+ primary ion beam and a 2nA or 600 pA Cs^+ primary ion beam rastering an area of 150 ×150 μm^2 respectively.

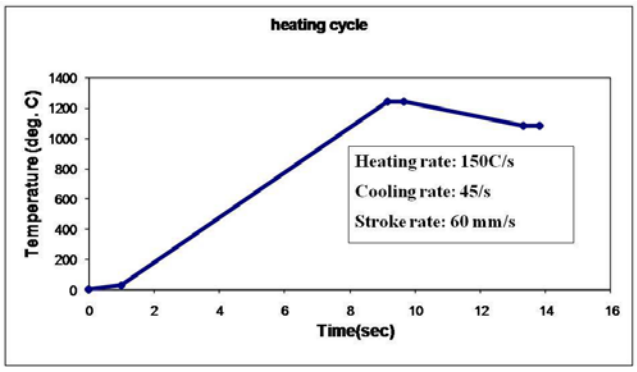

Figure1: Typical Gleeble thermal cycle

Cracking susceptibility of the welds was determined by measuring crack lengths in 10 sections cut in a direction transverse to the weld using SEM image analysis software. The hot ductility tests were conducted with a Gleeble 1500-D thermo-mechanical simulation device using cylindrical specimens of diameter 10 mm and length 158 mm. The "on-heating" and "on-cooling" hot ductility tests were performed in air to simulate the welding thermal cycle. During on-heating tests, the samples were heated to the test temperature at a heating rate of 150°C/s, held there for 0.5s for stabilization, and then tensile stressed to fracture. During on-cooling ductility tests, the samples were heated to a peak temperature (T_p) of 1200°C and then controlled cooled at 45°C/s to the test temperatures. The cooling rate of 45°C/s was recommended by Lundin et.al.[13, 14] in their article published on standardization of Gleeble parameters and falls well within the range of experimentally measured cooling rates determined by thermocouples embedded in the HAZ[15, 16]. After holding for 0.5s, tensile stress was applied to fracture the sample. The test parameters are summarized in Table 2 and a typical Gleeble thermal cycle is shown in Figure 1. The hot ductility of the alloys at different test temperatures was determined from the reduction in area of the specimens, which was obtained by measuring the initial diameter and the final diameter of the fractured specimen. The material parameters measured were: on-heating nil ductility temperature (NDT), on-cooling ductility recovery temperature (DRT), and the brittle temperature range (BTR), which is the temperature range between Tp and DRT.

Table 1: Chemical Composition of the Alloys

wt %	Inconel 718	Allvac 718 Plus **(HC 49)**	Allvac 718 Plus **(HC 20)**
Ni	54.44	52.21	52.18
Cr	17.94	17.42	17.92
Fe	17.62	9.66	9.33
Co	0.13	9.13	9.00
Nb	5.36	5.48	5.51
Ti	0.94	0.71	0.74
Al	0.46	1.46	1.50
B	0.004	0.005	0.003
P	0.007	0.013	0.006
C	0.026	0.028	0.022
Mo	2.93	2.72	2.68
W	<0.01	1.04	1.04
S	<0.0003	<0.0003	<0.0003
Si	0.05	0.05	0.02

Table 2: Gleeble parameters used in this study

Sample dimensions	10 mm dia, 158 mm length
Free Span	50 ± 2 mm
Heating rate	150 °C/s
Hold time at test temperature	0.05 s
Hold time at peak temperature	0.05 s
Stroke rate	60 mm/s
Cooling rate	45°C/s
Peak Temperature	1200°C

Results

Microstructural Analysis

Solution heat treated condition: The microstructure of HC-20 718 Plus alloy, heat treated at 950°C for 1 hour had a grain size of 54 ±6 μm with few randomly dispersed phases. As shown in Figure 2, needle like δ phase was observed on the grain boundaries, and occasionally intra-granularly on the twin boundaries. Due to the thin needle-shaped morphology of δ phase, it was difficult to accurately determine its chemical composition without eliminating the contribution from the matrix elements. The composition as determined by high resolution TEM EDS Inca software is reported in Table 3. Also seen in the microstructure were randomly distributed, round and blocky shaped MC type carbide particles. SEM EDS analysis revealed them to be rich in Nb and Ti. Some of the carbide particles were also enriched in boron as shown in the EDS x-ray analysis spectrum shown in Figure 3. Ti-rich carbo-nitride particles were also observed in the microstructure (Figure 2). Intermetallic phases like FCC γ′ and

BCT γ″ are expected to form in 718 Plus alloys but γ′ is the main strengthening phase in these superalloys [6]. TEM analysis revealed the presence of spherical γ′ particles, shown in a dark field image, Figure 4, which was obtained with the γ′ superlattice reflections of γ′ shown in the selected area diffraction pattern (SADP) obtained in a direction parallel to [001] zone axis, shown in the inset of Figure 4. This suggests that standard solution heat treatment at 950°C for 1 hour only resulted in a partial dissolution of the principal strengthening phase. SADPs in the direction parallel to [001] should also show the (0 1/2 0) type superlattice reflections corresponding to γ″ phase if it were to be present [17], however, they were not observed. Absence of these superlattice reflections suggests that γ″ particles were not present in this heat treated condition.

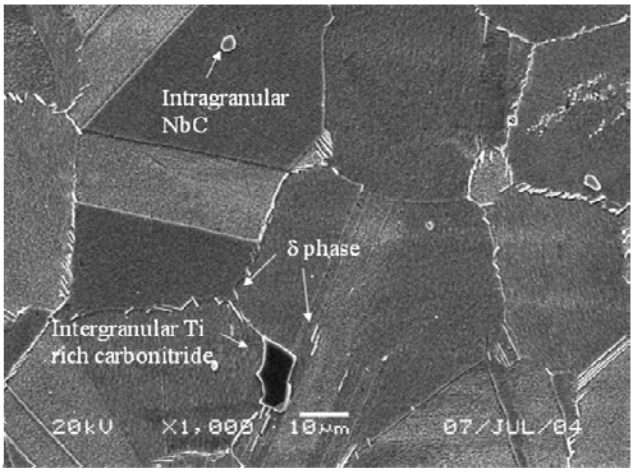

Figure 2: Microstructure of HC 20 718 Plus alloy after 950°C heat treatment

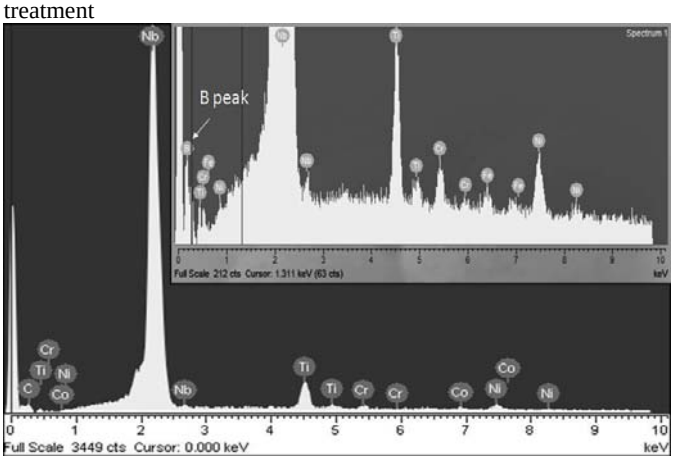

Figure 3: SEM X-ray EDS spectrum corresponding to Nb rich MC type carbide showing boron peak

Similar microstructural features were observed in high boron and phosphorus version of 718 Plus alloy, HC-49. Interestingly, the microstructure of Inconel 718 was also very similar to that of the 718 Plus alloy except for the absence of γ′ particles. Unlike 718 Plus alloy, Inconel 718 is primarily strengthened by BCT γ″ phase and partly by FCC γ′ phase. The standard solution heat treatment at 950°C is above the solvus of γ′ and γ″ in Inconel 718 [18], hence they were not observed.

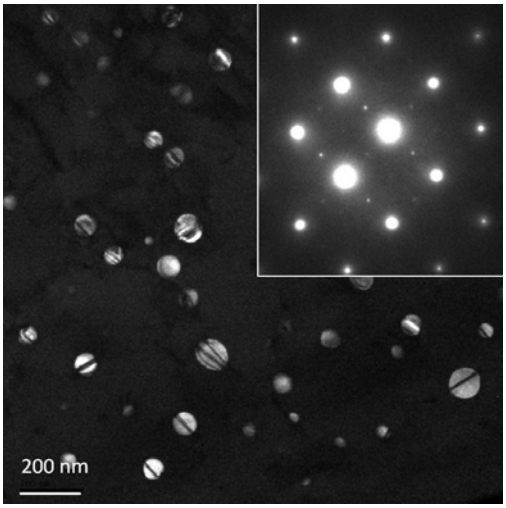

Figure 4: High resolution transmission electron dark field image of spherical γ′ particles observed in 950°C solution heat treated HC 20 718 Plus alloy. Inset shows an SADP in [001] direction with superlattice reflections corresponding to γ′ particles while superlattice reflections due to γ″ particles were not observed

Table 3: Average chemical composition of various phases in HC-20-718 Plus alloy as determined by TEM/EDS x-ray analysis

Elements wt%	Delta phase (HRTEM)	Nb-rich carbides-fusion zone (TEM)	Laves phase – fusion zone (TEM)	Laves phase – fusion zone [7][7] (TEM)
Al	1.89	–	1.15	0.56
Ti	3.02	5.27	0.90	1.9
Cr	3.03	2.84	10.95	12.8
Fe	5.63	1.30	5.35	13.6
Co	5.22	1.83	7.55	–
Ni	62.37	5.83	34.00	46.5
W	-	–	2.90	–
Nb	22.27	81.76	31.65	21.2
Mo	-	3.68	5.65	3.6
V	-	–	–	–
Si	-	–	–	0.78

Microstructure of the three alloys after solution heat treatment for 1 hour at 1050°C was essentially the same. Dissolution of δ phase resulted in almost a single phase material with a few randomly distributed carbide particles. The amount and distribution of carbides and carbo-nitrides was not significantly affected by the heat treatment. 1050°C heat treatment resulted in a complete dissolution of γ′ phase and no superlattice reflections were observed in the SADPs in the [001] zone axis, an example of which is shown in Figure 5.

Welded microstructure:

EB bead-on-plate autogenous welds were made on the solution heat treated alloys, which had a typical partial penetration nail head weld profile, as shown in Figure 6. None of the alloys, in either of the two heat treated conditions exhibited fusion zone cracking. Cracking was confined to the HAZ and predominantly occurred under the nail head, in the shoulder region.

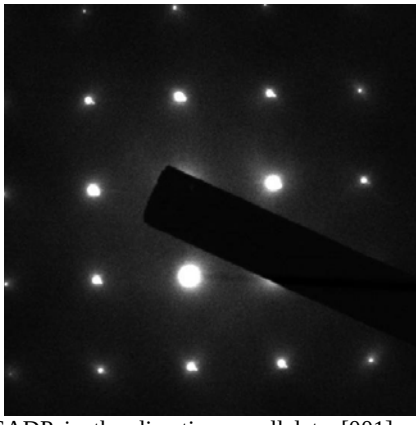

Figure 5: SADP in the direction parallel to [001] axis with no superlattice reflections corresponding to γ′ or γ″ particles

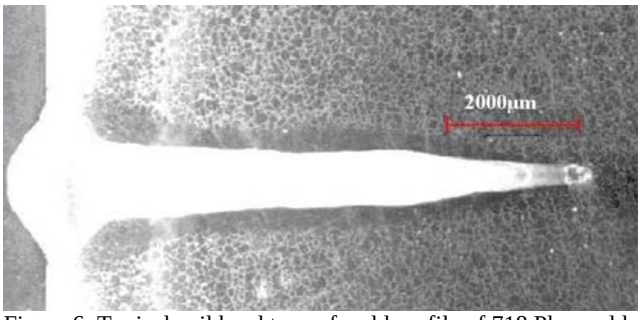

Figure 6: Typical nail head type of weld profile of 718 Plus welds

Fusion zone of HC-20-718 Plus alloy had a fine cellular dendritic structure as shown in Figure 7. The micro-segregation analysis indicated that during solidification of the fusion zone Fe, Co, W and Cr segregated to the core of the gamma dendrites, and Nb, Ti and Al were extensively rejected into the interdendritic liquid [19]. A typical TEM bright field image of one of the two major particles observed in the thin foils made from the fusion zone, and its associated TEM/EDS spectrum are shown is Figure 8. The spectrum suggests that the particle contained predominantly Nb and smaller amounts of other elements (Figure 8b). The chemical composition of these particles (Table 3) was similar to that observed of face centered cubic NbC particles with lattice parameter of a = 0.454nm. Therefore, these particles were identified to be Nb rich MC type carbides. Other particles observed on the carbon extraction replicas and in thin foils prepared from the fusion zone had an irregular shape and exhibited faulted structure, and were identified as Laves phase. A bright field image of one such particle is shown in Figure 9a. TEM/EDS analysis of Laves phases revealed them to be enriched in Nb, Mo and Ni (Figure 9b) and the average chemical composition of these particles is listed in Table 3.

Gamma prime particles were not observed by TEM examination of thin foils made from the fusion zone of the welds, as concluded after analysis of the SADP obtained in [001] orientation by JEOL 2100 FX field emission high resolution TEM, Figure 10. If γ′ particles were to be present this SADP would contain (001), (100) or (010) type of superlattice reflections. There absence indicates that γ′ precipitates did not form in the fusion zone of the welds.

HAZ Microstructure and Micro-fissuring:

It was observed that grain boundaries in HAZ adjacent to the fusion zone were liquated and re-solidified forming a partially melted region. Besides grain boundary liquation, inter- and intra-granular liquation of NbC particles was observed in the HAZ (Figure 11). Figure 12 shows a back scattered electron SEM image of HAZ micro-fissure in HC-20-718 Plus alloy. As can be seen, cracking originated a small distance away from the fusion zone and was always intergranular in nature. Cracks were also associated with re-solidified products suggesting liquation type of cracking in these alloys. Some of the cracks were backfilled by the liquid from the fusion zone, which resulted in a partial healing of the cracks. The re-solidified products on the backfilled grain boundaries and around the cracks were identified as Laves/γ eutectic (Figure 13). Carbon extraction replicas prepared by masking the fusion zone and the base metal also revealed the presence of NbC/γ eutectic, an example of which is shown in Figure 14. SADP taken in a [001] direction from one such NbC particles is shown in the inset of Figure 14. The chemical composition and lattice parameter of these carbides were similar to that observed in the fusion zone and the base-metal.

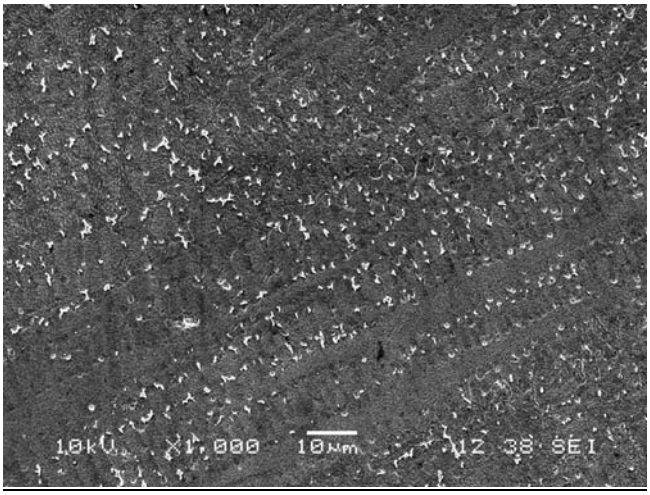

Figure 7: Fusion zone microstructure of HC 20 718 Plus alloy

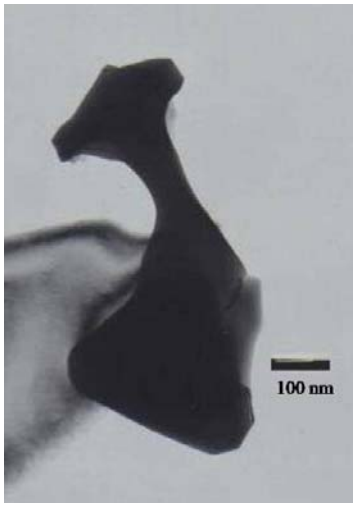

Figure 8: (a) Bright field image of NbC particle observed in the fusion zone of HC 20 718 Plus alloy

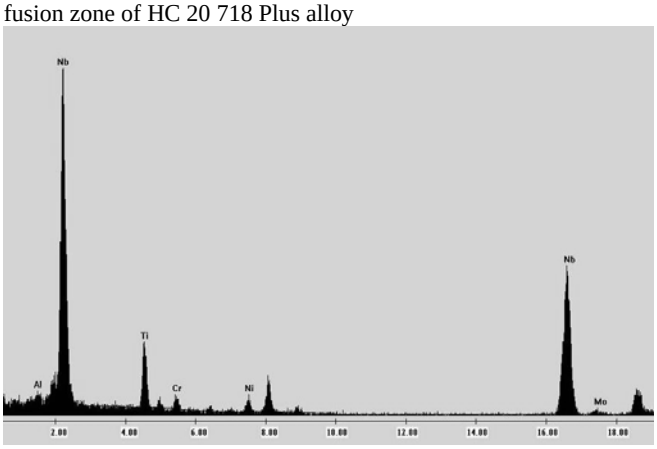

Figure 8 (b) TEM/EDS spectrum associated with the particle

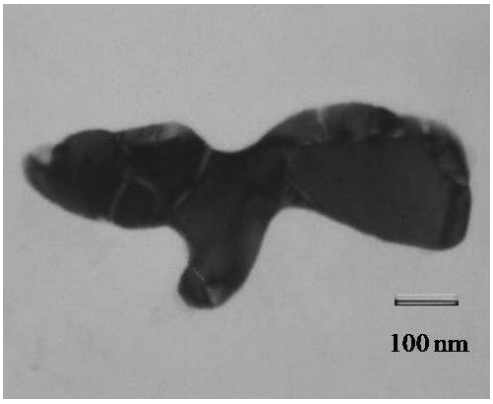

Fig. 9a

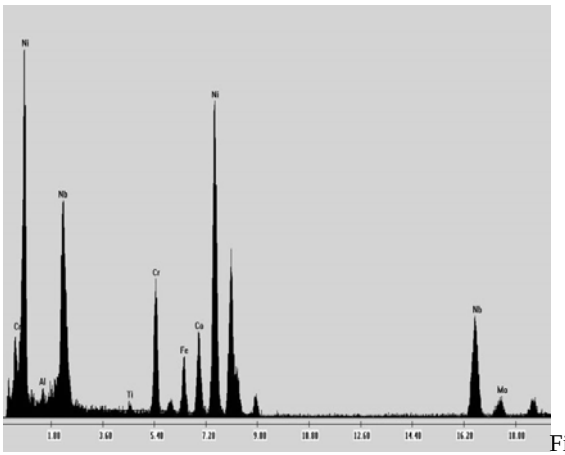

Fig. 9b

Figure 9: (a) Bright field image of Laves phase found in the fusion zone of HC 20 718 Plus alloy (b) TEM/EDS spectrum associated with the Laves phase

The micro-fissuring observed in HC-49 and Inconel 718 was similar to that observed in HC-20 718 Plus alloy. Also, morphologically and metallurgically, micro-fissuring observed in both the heat treated conditions in all the three alloys was similar. Although, the amount of cracking amongst the alloys and in the two heat treated conditions was different, and is compared in the discussion section.

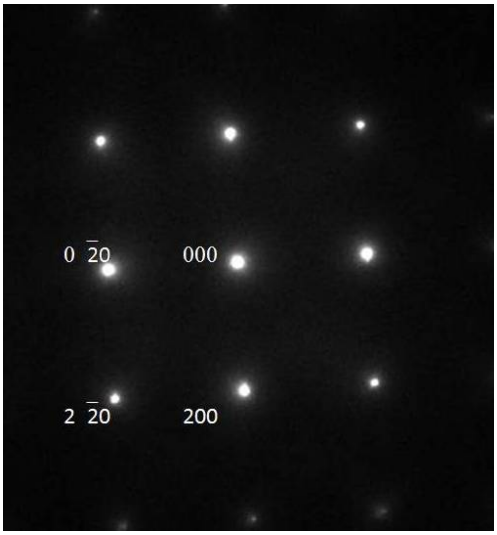

Figure 10: SADP of the matrix in [001] orientation, showing absence of γ' superlattice reflections.

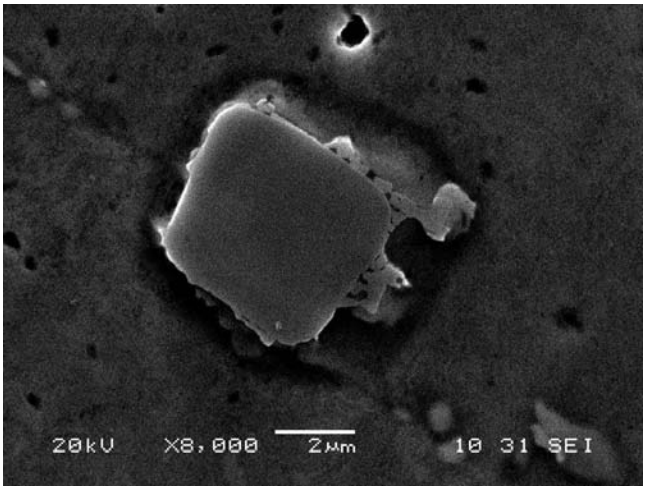

Figure 11: Constitutionally liquated Nb rich MC type carbide particle in the HAZ of HC 20-718 Plus alloy

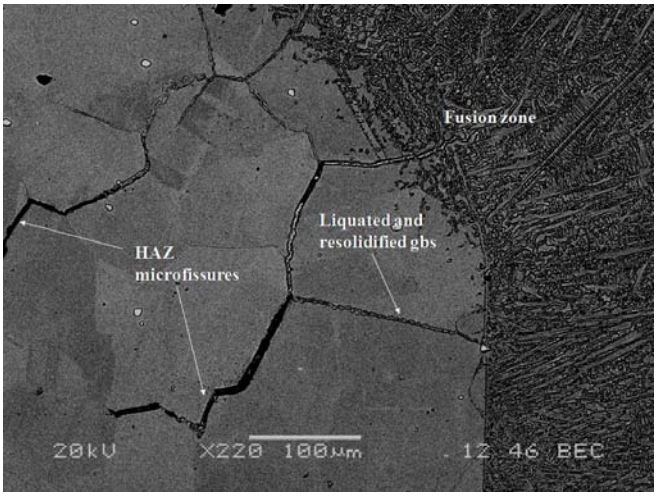

Figure 12: HAZ microfissuring in HC 20-718 Plus alloy

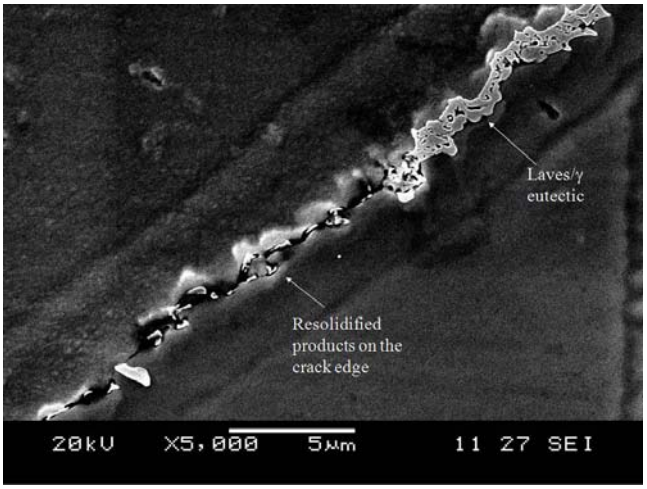

Figure 13: Resolidified Laves/γ eutectic type products on the liquated and cracked grain boundaries

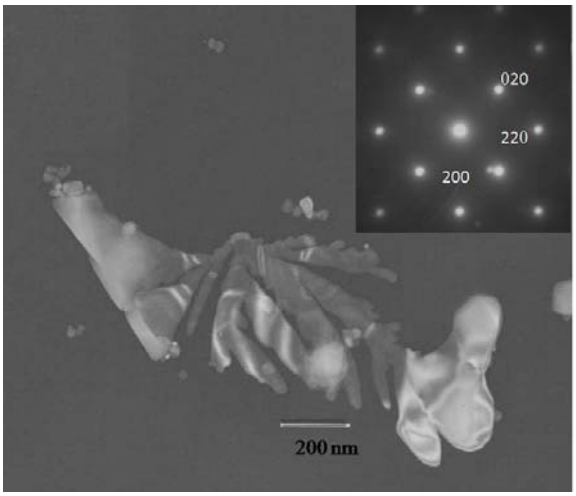

Figure 14: (a) Resolidified NbC particle extracted from the HAZ of HC 20 718 Plus alloy (b) SADP of NbC particle in the direction parallel to [001] zone axis

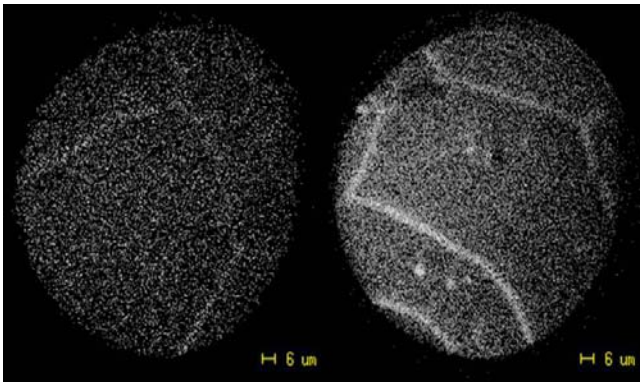

Figure 15: Boron ion SIMS image in the 1050°C heat treated condition (a) in HC 20 (b) in HC 49

SIMS Analysis:

Grain boundary segregation of boron and phosphorus was studied in HC-20 and HC-49 718 Plus alloys. SIMS analysis did not reveal any segregation in either of the alloys in the 950°C heat treated condition, however some segregation of boron was observed in the 1050°C pre-weld heat treated condition. As can be seen in Fig. 15, the boron ion images of HC-49 alloy in the 1050°C heat treated condition was marginally stronger than in the HC-20 718 Plus. This indicates a greater degree of B segregation in HC-49 (with higher B and P) alloy than in HC-20 alloy. Phosphorus segregation was not revealed in either of the two pre-weld heat treated conditions. Analysis of the welds in the 1050°C condition showed boron and phosphorus segregation on the micro-fissured and re-solidified grain boundaries. Figure 16 shows segregation of boron and phosphorus on a micro-fissure in HC-20 alloy. Similar segregation was observed in HC-49-718 Plus alloy.

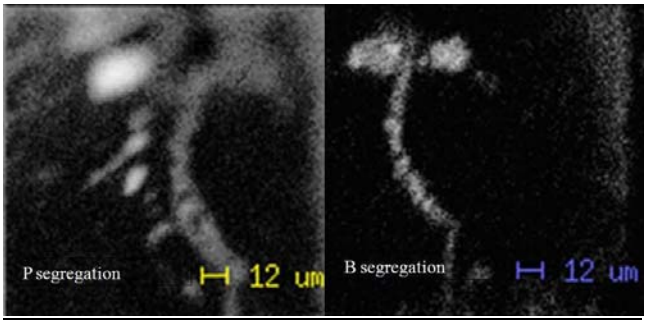

Figure 16: (a) Boron ion image (b) Phosphorus ion image at a liquation crack in HC 20 718 Plus alloy

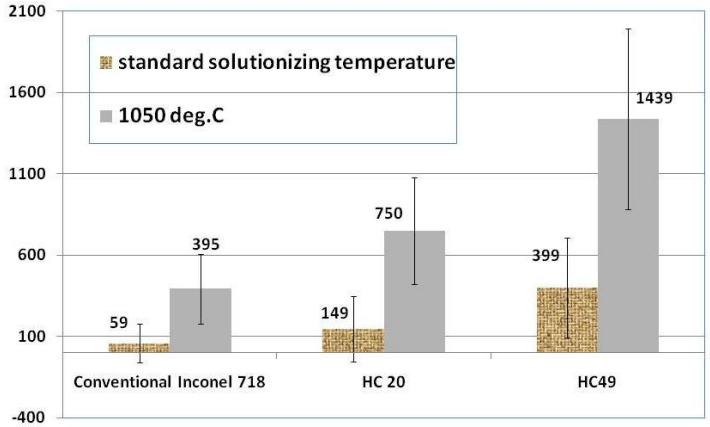

Figure 17: Average total crack length in Inconel 718 and 718 Plus alloys in the two pre-weld heat treatment conditions

Weldability Analysis:

Weld cracking:

The crack lengths were measured in 10 metallographic sections in the transverse direction to the weld. Total crack length (TCL) and maximum crack length were determined and an average total crack length per section was calculated. These values along with the standard deviation are listed in Table 4. A bar graph illustrating the values of average total crack length per section, in the two pre-weld heated conditions is shown in Figure 17. High variability was observed in total crack length for all cases, such that standard deviations partially overlapped for each heat treatment. It is seen that Inconel 718 is less susceptible to cracking than 718 Plus alloys in both the heat treated conditions. In material with a standard solution heat treatment at 950°C, cracking was least in Inconel 718, followed by the lower B and P

718 Plus HC-20, and was highest in the higher B and P alloy HC-49. A similar trend was observed after the solution heat treatment at 1050°C. Cracking in all the alloys increased considerably, more than by a factor of 4, with an increase in the solution heat treatment temperature. In 718 Plus alloys, cracking in the higher B and P version, HC-49, was almost twice the amount observed in the lower B and P alloy, in both the pre-weld heat treated conditions.

Table 4: Weld crack length in Inconel 718 and 718 Plus alloys

Alloys	Standard commercial solution heat treatment - 950°C/1hr + WQ*		
	Total crack length (μm)	Total Average crack length (μm)	Maximum crack length (μm)
Inconel 718	590	59 ± 119	72
HC 20 718 Plus	1490	149 ± 201	327
HC 49 718 Plus	3990	399 ± 307	253
	1050°C/1hr + WQ		
	Total crack length (μm)	Total Average crack length (μm)	Maximum crack length (μm)
Inconel 718	3950	395 ± 214	373
HC 20 718 Plus	7500	750 ± 330	468
HC 49 718 Plus	14390	1439 ± 557	419

Gleeble hot ductility measurements

Hot ductility is often used to evaluate a material's susceptibility to HAZ micro-fissuring. Inter-granular micro-fissuring in HAZ occurs due to liquation of grain boundaries by constitutional liquation of grain boundary precipitates or due to segregation of melting point depressant elements on them. The liquated grain boundaries reduce the ductility of the material to almost zero and the material is unable to withstand the welding stresses, resulting in the formation of intergranular micro-fissures. Therefore, the weldability of a material can be related to its ductility at higher temperatures, which can be measured by Gleeble thermo mechanical simulator.

Inconel 718 and the two 718 Plus alloys were heated at a rate of 150°C/s to different test temperatures and then tensile-stressed to fracture. The reduction in cross-sectional area of the samples was measured and plotted against the test temperature, as shown in Figure 18. The on-heating ductility curves of all the three alloys were very similar, and their nil-ductility values (NDT) were within 10°C of each other (Table 5). Inconel 718 had the lowest NDT of 1160°C, followed by HC-20-718 Plus of 1165°C, while the higher B and P alloy HC-49-718 Plus had the highest NDT of 1170°C. However, the observed minor difference in the NDT values is likely to be within the statistical scatter, and may not be significant.

The on-cooling tests were performed after heating the specimens of the three alloys to a peak temperature of 1200°C. A specimen heated to a peak temperature (T_P) essentially represents that portion of the HAZ material that experiences this temperature during the heating cycle of actual welding. For a better understanding of the HAZ micro-fissuring, temperatures higher than the temperature where grain boundary liquation starts are selected as T_p. Although some researchers have encountered grain boundary liquation at NDT, the values of T_P temperatures are generally selected to be higher than NDT. In the present case, the peak temperature was more than 25°C higher than the NDT values of the all the three alloys. As the NDT values were very similar, the same T_p was used for all the alloys, which yielded a better comparison of their hot ductility behavior. The values of on-cooling ductility are plotted in Figure 19. Unlike on-heating values, on-cooling ductility curves of each alloy were found to be considerably different, and the results are also listed in Table 5. Inconel 718 recovered its ductility at 1065°C on cooling from 1200°C, which yields a brittle temperature range (BTR) of 135°C (Figure 19). HC-20-718 Plus had a DRT of 1055°C, with a BTR of 145°C. The biggest BTR, 190°C, was observed in HC-49-718 Plus, with a DRT of 1010°C. These results indicate that Inconel 718 has a better on-cooling hot ductility as compared to that of either of the two 718 Plus alloys. It is to be noted that hot-ductility value of HC-20-718 Plus was only marginally worse than that of Inconel 718. Of the two 718 Plus alloy, DRT value of the higher B and P alloy, HC-49, was 45°C less than that of the lower B and P alloy. Similarly the BTR range of the higher B and P alloy was larger than that of the lower B and P alloy.

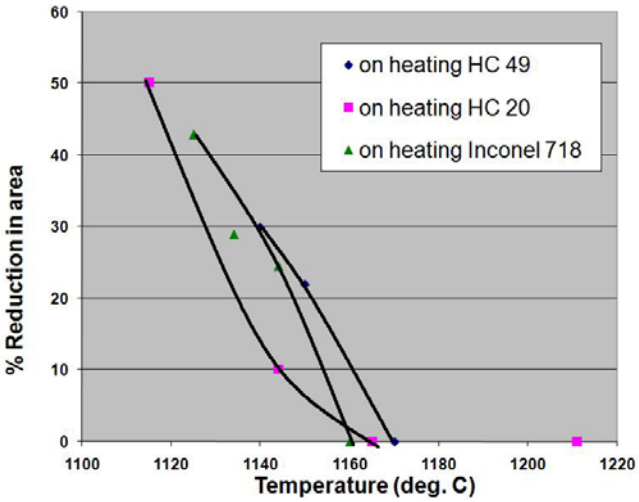

Figure 18: On-heating hot ductility values of Inconel 718, HC 20 718 Plus and HC 49 718 Plus alloy

Table 5: Hot ductility testing parameters for Inconel 718, HC 20 718 Plus and HC 49 718 Plus

Material	NDT	DRT	BTR = 1200°C – DRT
Inconel 718	1160	1065	135
Low B+P HC 20	1165	1055	145
High B+P HC 49	1170	1010	190

Discussion

The chemistry of 718 Plus alloy was modified considerably to obtain a 55°C working temperature advantage over the parent alloy, Inconel 718. The major changes included changing the aluminum to titanium ratio, replacing half of the iron content with cobalt and increasing the boron and phosphorus concentrations. A

change in aluminum to titanium ratio changed the main strengthening phase from γ″ in Inconel 718 to γ′ in 718 Plus alloys. Gamma prime particles were observed after the standard

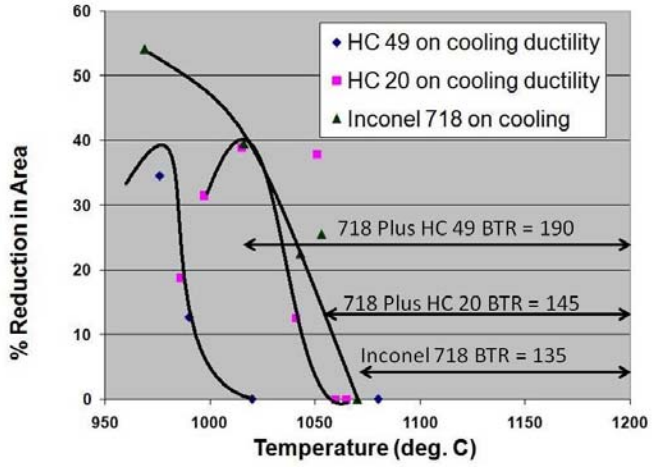

Figure 19: Variation in on-cooling hot ductility data of the three alloys with temperature with their BTRs

solution heat treatment in this study, which further suggests that, the solvus temperature of γ′ in 718 Plus alloy matrix, is higher than that observed in Inconel 718. Another important observation made in this study was the absence of γ′ particles in the weld fusion zone, which is unlike other γ′ strengthened superalloys. This suggests that the rate of precipitation of γ′ during cooling after welding is slower in 718 Plus alloy and might be due to partitioning of Nb in the particle. Other than γ′, most of the other phases viz. NbC carbides, TiN and Laves phases were also found in Inconel 718. The chemical composition of these phases was also comparable except for Laves phase composition. Laves phase in 718 Plus contained significantly smaller amounts of Fe than that observed in the Laves phase present in Inconel 718, whereas it was rich in Co which was not present in the latter. Interestingly, the total amount of Fe and Co in 718 Plus is approximately equal to the Fe content in Inconel 718. In addition, Nb concentration in the Laves phase in 718 Plus was observed to be greater than that generally observed in Inconel 718, while the reverse was true for the Ni concentration. Average chemical compositions of Laves phases found in Inconel 718 [7] and as determined in this study are listed in Table 3 for comparison.

In spite of these compositional differences, the development of microstructure during welding and the solidification sequence observed in the fusion zone and in liquated portions of the HAZ were remarkably similar in the two alloys. Accordingly, the first solid to form from the solidifying liquid were γ dendrites. The elements with partition coefficient less than unity (Nb, Al, etc.) partitioned into the solidifying liquid. When the solubility of Nb and C in the liquid is exceeded γ/NbC eutectic reaction would begin, which would continue to occur over a temperature range via a non-invariant reaction. The terminal eutectic reaction occurs in the form of γ/Laves reaction. This solidification sequence was observed in the fusion zone and in the liquated /backfilled grain boundaries in the HAZ of both the alloys.

Grain boundary segregation:

Grain boundary segregation influences the formation and stability of the intergranular liquid that may form during the welding thermal cycle. Segregation of minor alloying elements or impurities can (i) reduce the melting point of the grain boundary material [12, 20] (ii) increase the wetting behavior of the liquid [10] (iii) form low melting compounds that dissociate during the welding thermal cycle [11]. The presence of elements like boron [11, 21, 22], sulphur [8, 23], carbon and phosphorus [7, 24] are known to adversely affect the weldability of superalloys.

Segregation at grain boundaries occurs either by 1) equilibrium or 2) non-equilibrium modes. Solute atoms in a solid solution have a tendency to segregate to the grain boundaries because their atomic mismatch with the matrix atoms can be more easily accommodated there as it reduces the free energy of the system. This is known as equilibrium segregation [25], and decreases with an increase in the solutionizing temperature [26]. Non-equilibrium segregation which occurs due to the formation of vacancy- solute complexes during the cooling of the alloy from the heat treatment temperature depends on the cooling rate from that temperature. Increase in the heat treatment temperature increases the number of vacancies exponentially and during cooling from this temperature, the solute-vacancy complexes diffuse to the grain boundaries which act as sink for the vacancies [22]. It was observed that when the pre-weld solution heat treatment temperature was increased from 950°C to 1050°C the segregation of B on the grain boundaries increased in both the alloys, as was revealed by SIMS. This suggests that the segregation was of non-equilibrium type.

The micro-fissures in HAZ exhibited a presence of boron and phosphorus on them suggesting co-segregation of these elements. In the present study, segregation of phosphorus was not observed in the pre-weld heat treated specimen, while it was observed only on edges of the cracks that formed on welding. It is likely that phosphorus segregation on grain boundary was too small to be detected in the pre-weld specimens. However welding caused liquation cracking and during solidification of the liquated boundaries, phosphorus, whose partition coefficient in nickel is less than unity, would be rejected by the solidifying liquid in the solidifying by-product. This would increase the concentration of phosphorus on the edges of the cracks and when it would reach a critical minimum value, phosphorus would be detected by SIMS, as was observed to be concentrated on the edges of the cracks filled with re-solidified products.

HAZ micro-fissuring was significantly enhanced in HC-49 718 Plus as compared to that observed in HC-20 718 Plus, which can be directly related to the grain boundary segregation of boron and phosphorus. HC-49 718 alloy with more boron and phosphorus exhibited greater segregation of boron than that was observed in HC-20. Boron and phosphorus both adversely influence weldability, which was also observed in a study on the effect of minor alloying elements on weldability of Inconel 718 by Benhadad.et.al [24] where the combined presence of B and P was found to be most detrimental.

Weld cracking measurements:

The values of the total average crack lengths indicated that micro-fissuring was least in Inconel 718, followed by HC-20-718 Plus and was highest in HC-49 718 Plus alloys, in both the heat treated conditions. Better cracking resistance of Inconel 718 compared to that of 718 Plus alloys can be attributed to lower base metal hardness of the alloy in either of the two heat treated conditions. Hardness values of all the three alloys before and after welding are listed in Table 5. In earlier studies on IN 738 LC superalloy welded with different filler alloys, the HAZ and fusion zone

micro-fissuring was related to the base metal hardness of the alloy [27, 28]. It was found that a lower base metal hardness improved alloy's resistance to micro-fissuring during welding. Softer base metal and better ductility of the alloy would allow the stresses developed during welding to be relieved in the softer base metal rather than the crack sensitive HAZ. As has been reported earlier, the microstructures of these alloys were very similar except for the presence of γ′ phase in the 950°C solution heat treated 718 Plus alloys. The hardness of 718 Plus alloys was about 75 VPN higher than that of Inconel 718 in the 950°C heat treated condition. Gamma prime phase was not observed in the 1050°C solution treated condition, nevertheless, the hardness of the 718 Plus alloys was higher than that of Inconel 718 by almost 50 VPN. Hence, Inconel 718 with softer base metal suffered a significantly reduced cracking compared to 718 Plus alloys, in spite of the apparent similarities in the microstructure.

HAZ micro-fissuring in all the alloys increased with an increase in the heat treatment temperature, which can also be attributed to the increase in grain size of the alloys. It has been reported that increasing grain size, independent of other variables, increased micro-fissuring susceptibility. A large grain size would have longer interface sliding length, larger stress concentrations and large strain at grain boundary triple points, all increasing the susceptibility to micro-fissuring [29]. In the present study, solution heat treatments were selected so that the variation in grain sizes between the alloys studied was minimum. Inconel 718 and 718 type alloys had very similar grain sizes after the two solution heat treatments. Another factor that may be affected by the increase in grain size is the grain boundary segregation of an element because as the grain size increases the total grain boundary area available for segregation to occur decreases. Faulkner's model for non-equilibrium segregation also predicted that grain size has an impact on non-equilibrium segregation; larger grain size leads to higher segregation intensity. As was observed, micro-fissuring in HC-49 718 Plus with higher boron and phosphorus was significantly higher in both the heat treated conditions, but it was maximum in the 1050°C heat-treated condition.

Hot ductility Measurements:

The hot-ductility behavior of Inconel 718 and HC-20 718 Plus alloy was very similar, with a very small brittle temperature range. This indicates that their susceptibility to HAZ micro-fissuring should also be very similar in the 950°C solution heat treatment condition. The weld cracking behavior of the two alloys, as was discussed earlier, indicated that HAZ cracking in Inconel 718 was one-third (59 μm) of the cracking observed in HC-20 718 Plus (149μm). The difference in the amount in cracking in the 950°C heat treated condition seems to be disproportionately higher than the difference in their BTRs, although the trend remained the same, with Inconel 718 showing better resistance to micro-fissuring.

A comparison between the two 718 Plus alloys exhibited a more discernible difference. While the on-heating ductility values were nearly the same, it was observed that higher amounts of boron and phosphorus significantly reduced the on-cooling hot ductility values, as indicated by the DRT values of both the alloys. The alloy with higher B+P concentration had a lower DRT value and a larger brittle temperature range (Table 5). This further suggests that intergranular liquid in the HC-49 would remain liquid to lower temperatures during cooling of the weld, which would make the alloy more susceptible to cracking. Boron has been known to affect the on-cooling hot ductility of Inconel 718 [12, 30], and a similar effect was observed in 718 Plus alloys. The presence of boron and phosphorus increased the solidification temperature range of 718 Plus alloys. This corroborates the weld cracking values where HC-49 718 Plus had a TCL of 399μm compared to 59μm in HC-20 718 Plus alloy.

Mechanisms of micro-fissuring in 718 Plus alloy:

Microstructural characterization and grain boundary segregation analysis suggested that the main mechanism of micro-fissuring in 718 Plus was liquation at grain boundaries in the HAZ. The two primary causes of liquation were identified as (1) constitutional liquation of NbC particles (2) grain boundary liquation due to segregation of minor alloying elements, boron and phosphorus. It was also observed that the amount and distribution of carbides/carbo-nitrides did not significantly change in the two pre-weld heat treated conditions; however, significant increase in micro-fissuring was observed. The increase in micro-fissuring thus correlated better with the increase in grain boundary segregation in 718 Plus alloys which, therefore, appears to be the dominating HAZ cracking mechanism.

Summary and Conclusions

1. Pre-weld microstructures of 718 Plus alloys and Inconel 718 after the 950°C heat treatment were similar except for the principle strengthening phase, which was γ′ in the two 718 Plus alloys. Other phases observed in the three alloys were grain boundary δ phase, NbC particles and Ti carbo-nitride particles. The 1050°C heat treatment dissolved the δ phase but did not significantly change the amount and distribution of the carbides/carbo-nitrides.

2. Fusion zone microstructure of all the alloys had fine cellular dendritic microstructure. Laves/γ eutectic and Carbides/γ eutectic phases formed in the interdendritic region.

3. Liquation cracking was observed in the HAZ of all the three alloys and was associated with re-solidified products. Though it was larger in 718 Plus alloys than that was observed in Inconel 718. The causes for liquation were identified as constitutional liquation of grain boundary NbC particles, grain boundary segregation of B and P.

4. B and P adversely affected the weldability of the 718 Plus alloys by increasing the solidification range during weld thermal cycle.

5. Average crack length and hot ductility measurements indicated that weldability of 718 Plus alloy with normal B and P concentration was marginally worse than that of Inconel 718. The susceptibility of the alloys to liquation cracking increased in the following sequence – Inconel 718 < HC-20 718 Plus < HC-49 718 Plus.

Acknowledgements

The authors would like to thank NSERC and the University of Manitoba for the financial support and ATI Allvac for providing the material for this research and valuable comments.

References

1. M.S.Prager and C.S.Shira, "Welding of Precipitation-hardening Nickel- base superalloys", *Weld. Res. Counc. Bull.*, 128 (1968).
2. E.G.Thompson, "Hot cracking studies of alloy 718 weld heat-affected zones*", Welding Journal*, 48(1969), pp.70s - 79s.
3. R.Cozar and A. Pineau, "Morphology of gamma prime and gamma double prime precipitates and thermal stability of Inconel 718 type alloys", *Metallurgical Transactions*, 4(1973), 47-59.
4. E.Guo, F. Xu, and E.A. Loria, "Effect of heat treatment and compositional modification on strength and thermal stability of alloy 718", *Superalloys 718, 625 and various derivatives*, (1991), 389-396.
5. D.Jianxin, X. Xishan, and Z. Shouhua, "Coarsening behavior of gamma double prime precipitates in modified Inconel 718 superalloy", *Scripta Metallurgica et materialia*, 33(1995), pp. 1933-1940.
6. W.D.Cao and R. Kennedy, "Role of chemistry in 718-type alloys - Allvac 718 Plus Alloy Development", *Superalloys 2004*, (2004), 91- 99.
7. N.L.Richards and M.C. Chaturvedi, "Effect of minor elements on weldability of nickel base superalloys", *International Materials Review*, 45(2000), 109 - 129.
8. H.Guo, M.C. Chaturvedi, and N.L. Richards, "Effect of sulphur on hot ductility and heat affected zone microfissuring in Inconel 718 welds", *Science and Technology of Welding and Joining*, 5(2000), 378-384.
9. S.R.Benhadad,et.al., "The influence of B, P and C on heat-affected zone micro-fissuring in Inconel Type superalloy", *Superalloys 2000*, 703-711.
10. W.F.Savage, E.F. Nippes, and G.M. Goodwin, "Effect of minor elements on hot cracking tendencies of Inconel 600", *Welding Journal*, 56(1977), 245s - 253s.
11. T.J.Kelly, "Elemental effects on cast 718 weldability", *Welding Journal*, (1989), 44s-51s.
12. H.Guo, M.C. Chaturvedi, and N.L. Richards, "Effect of boron concentration and grain size on weld heat affected zone microfissuring in Inconel 718 base superalloys", *Science and Technology of Welding and Joining*, 4(1999), 257-264.
13. Lundin, C.D., C.Y.P. Qiao, and C.H. Lee, *Standardization of gleeble hot ductility testing: Part1: Historical review*. Weldability of Materials, Detroit, Michigan, USA, (1990), 1-9.
14. C.D. Lundin, C.Y.P. Qiao, and C.H. Lee, *Standardization of Gleeble hot ductility testing: Part II: Experimental Evaluation*, Weldability of Materials, Detroit, Michigan, USA, (1990), 9-22.
15. Carin, M., et al., *Experimental validation of a predictive model for numerical simulation of thermo-metallurgical phenomena during electron beam welding.* Journal of Physics IV France, (2004), 120, 599-606.
16. H.J.Stone, S.M. Roberts and R.C. Reed, , *A process model for the distortion induced by the electron-beam welding of a nickel-based superalloy*, Metallurgical and Materials Transactions A, 2000, (2000), 2261-2273.
17. D.F.Paulonis, J.M. Oblak, and D.S. Duvall, "Precipitation in Nickel base Alloy 718", *Transactions of American Society of Metals*, 62(1969),611-622.
18. J.F.Radavich, "The physical metallurgy of cast and wrought Alloy 718", *Superalloy 718 - Metallurgy and Applications*, (1989), 229-240
19. K.Vishwakarma and M.C. Chaturvedi, "Characterization of Fusion Zone and Heat Affected Zone Microstructures of Electron beam welded Allvac 718 Plus alloy", *Article in press, Materials Science and Engineering*, 2007.
20. W.A.Owczarski, D.S. Duvall, and C.P. Sullivan, "A model of HAZ cracking in Nickel - base superalloys", *Welding Journal*, 45 (1966), 145s – 155s.
21. W.Chen, N.L.Richards and M.C.Chaturvedi, "Grain boundary segregation of boron in Inconel 718", *Metallurgical and Materials Transactions A*, 29A (1998), 1947 - 1954.
22. X.Huang, N.L.Richards and M.C.Charurvedi., "The effect of grain boundary segregation of boron in cast alloy 718 on HAZ microfissuring - A SIMS analysis", *Acta materialia*, 45 (1997), 3095 - 3107.
23. R.G.Thompson, M.C. Koopman, and B.H. King, "Grain Boundary Chemisty of Alloy 718 - Type Alloys", *Superalloys 718, 625, and Various Derivatives*, (1991), 53-70.
24. S.Benhadad, N.L. Richards, and M.C. Chaturvedi, "The influence of minor elements on the weldability of an Inconel 718 type superalloy", *Metallurgical and Materials Transactions A*, 33A (2002), 2005-2017.
25. D.McLean, *Grain boundaries in Metals*. 1957, Oxford: Clarendon Press.
26. X.Huang, M.C. Chaturvedi, and N.L. Richards, "Effect of homogenization heat treatment on the microsturcture and heat-affected zone microfissuring in welded cast alloy 718", *Metallurgical and materials Transactions A*, 27 A (1996), 785-790.
27. R.K.Sidhu, N.L. Richards, and M.C. Chaturvedi, "Effect of aluminium concentration in filler alloys on HAZ cracking in TIG welded cast Inconel 718LC superalloy", *Materials Science and Technology*, 21 (2005), 1119 - 1131.
28. K.Banerjee, N.L. Richards, and M.C. Chaturvedi, "Effect of Filler Alloys on Heat-Affected Zone Cracking in Preweld Heat-Treated IN-738 LC Gas-Tungsten-Arc Welds", *Metallurgical and Materials Transactions A*,36A(2005), 1881 -1890
29. R.G.Thompson, et al.,"The relationship between grain size and microfissuring in Alloy 718", *Welding Journal*, 64,(1985), 91s- 96s.
30. H.Guo, N.L.Richards and M.C.Chaturvedi, "Interdependence of character of grain boundaries, inter-granular segregation of boron and grain boundary liquation in simulated weld heat- affected zone in Inconel 718", *Scripta materialia*, 40 (1999), pp. 383-388.